Electrochemical and Computational Investigations on the Corrosion Inhibition of X65 Steel by 2-Phenylbenzimidazole in H₂SO₄ Solution

Jianhong Tan[1], Lei Guo[2,3], Dan Wu[1], Xuejing Duan[1], Senlin Leng[2], Ime Bassey Obot[4], Savaş Kaya[5]*

[1] School of Chemistry and Chemical Engineering, Yangtze Normal University, Chongqing 408100, China
[2] School of Material and Chemical Engineering, Tongren University, Tongren 554300, China
[3] Material Corrosion and Protection Key Laboratory of Sichuan province, Sichuan University of Science and Engineering, Zigong 643000, China
[4] Center of Research Excellence in Corrosion, King Fahd University of Petroleum and Minerals, Dhahran 31261, Saudi Arabia
[5] Department of Chemistry, Faculty of Science, Cumhuriyet University, Sivas 58140, Turkey
[*]E-mail: cqglei@163.com

In this work, we studied 2-phenylbenzimidazole (PBI) as a corrosion inhibitor for X65 steel in H₂SO₄ medium. The inhibition performance of PBI for X65 steel were studied using weight loss, electrochemical experiments, surface analysis and computational modelings. The results indicate that PBI has a superior anti-corrosion performance and belongs to modest cathodic-type corrosion inhibitor. The adsorption behavior of PBI molecule on steel conforms to Langmuir adsorption model. The adsorption type is a combination of physical and chemical adsorption. SEM morphology analysis can prove inhibition performance of PBI. DFT calculation and molecular dynamics simulations have revealed active adsorption sites and adsorption configuration of PBI molecule on Fe substrate.

1. INTRODUCTION

Corrosion inhibition of metal materials is considered as a challenging research area owing to its impact on economic and safety issues [1, 2]. X65 steel is one of the most important metal materials and is widely used in marine, construction, mechanical engineering, and military because of its good mechanical and structural properties, as well as high versatility. However, it is susceptible to corrosion

in working environment such as H_2SO_4 medium [3, 4]. Corroded steel poses a potential threat to the economic losses and personal safety.

To effectively reduce the corrosion of X65 steel, scientists have developed and many corrosion protection methods [5-8]. Among them, organic compounds containing heteroatoms are deemed as effective corrosion inhibitors for acid solution [9, 10]. They can adsorb onto the metal surface and a dense and ordered molecular barrier film is formed on the surface of metal [11-13]. Thus, the corrosion of metal can be inhibited effectively.

However, most of the organic inhibitors now are expensive and hazardous to environment and human, which prompt corrosion researchers to develop the alternative inexpensive and ecofriendly corrosion inhibitors [14-17]. In this study, an eco-friendly imidazole derivative, 2-phenylbenzimidazole (PBI) have been investigated as a new corrosion inhibitor for X65 steel in sulfuric acid solution. The molecule structure of PBI are shown in Figure 1, the benzene ring may strength the adsorption ability of imidazole molecule. The electrochemical tools, surface morphology analysis, weight loss method, Langmuir model, DFT calculation, and molecular dynamics (MD) simulation have been used to study the inhibition performance and mechanism of PBI. The theoretical modeling support the various experimental results well.
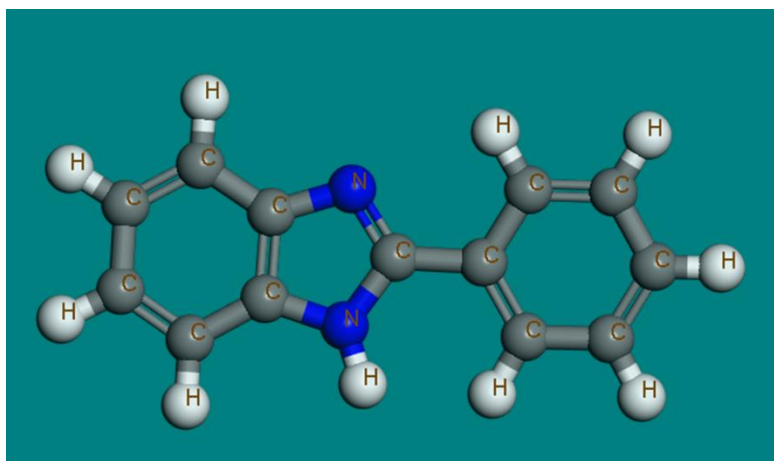
Figure 1. Molecular structure of PBI.

2. EXPERIMENTAL

2.1. Materials

The compound PBI was purchased without further purification. The selected X65 steel has a composition (wt.%) of C:0.65%, Si:0.26%, Mn:1.10%, P:0.019%, S:0.002%, Cr:0.02%, Ni:0.01%, Cu:0.01%, and balance Fe. The 0.5 M H_2SO_4 medium was treated as blank solution. Different concentrations (0.5 mM, 1 mM, 2 mM, 5 mM) of PBI in blank solution was prepared. Water bath was used to control experimental temperature.

2.2. Weight loss

Gravimetric experiments were performed by immersing steel in 0.5 M H_2SO_4 with different concentrations of PBI for 6 h at 298 K. The corrosion rate (CR), inhibition efficiency (v) and inhibition performance (η) can be calculated,

$$v = \frac{W_0 - W}{St} \qquad (1)$$

$$\eta(\%) = \frac{v_0 - v}{v_0} \times 100 \qquad (2)$$

where S the area of specimen, t represents immersion time, W_0 and W are the samples weight before and after exposure in corrosive solution, v_0 and v are the corrosion rates in the absence and presence of PBI respectively.

2.3. Electrochemical experiments

CHI 660E electrochemical station was used to perform the tests at 298 K. The electrochemical cell consists of a three-electrode system including a reference electrode, a working electrode and an auxiliary electrode. X65 steel were utilized as the working electrode, saturated calomel electrode (SCE) was reference electrode, and Pt was the counter electrode, respectively. EIS was recorded at an OCP within 100 kHz to 0.01 Hz with 5 mV signal. Polarization was measured over ±250 mV range of OCP at 2 mV/s sweep rate. The inhibition efficiencies are calculated as follows,

$$\eta_{EIS}(\%) = (1 - \frac{R_{ct,0}}{R_{ct}}) \times 100 \qquad (3)$$

$$\eta_{Tafel}(\%) = (1 - \frac{i_{corr}}{i_{corr,0}}) \times 100 \qquad (4)$$

where $R_{ct,0}$ and R_{ct} were charge transfer resistances in blank and inhibitor containing solution, $i_{corr,0}$ and i_{corr} were current densities of in blank and inhibitor containing solution, respectively.

2.4. Surface examination

Surface morphology of steel sample immersing in test solution in the absence and presence of 5 mM PBI was observed at scanning electron microscope (SEM, JEOL-JSM-7800F).

2.5. Calculation methods

Both quantum chemical calculation and molecular dynamics simulation (MDS) are effective ways to predict corrosion inhibition performance corrosion inhibition of corrosion inhibitor. In this study, DNP/PBE based on density functional theory (DFT) was used to predict the chemical activity of PBI molecule. The optimized frontier molecular orbital and important parameters were obtained. The interaction between PBI and Fe (110) surface were studied by Molecular dynamics simulation (MDS)

by Forcite-COMPASS-NVT canonical ensemble. This process is in a periodic boundary condition. The interaction and binding energies of PBI on Fe (110) surface were calculated [18]:

$$E_{int\,eract} = E_{tot} - (E_{subs} + E_{inh}) \quad\quad\quad (5)$$
$$E_{binding} = -E_{int\,eract} \quad\quad\quad (6)$$

where E_{tot} is total energy, E_{subs} is substrate energy, and E_{inh} stands for PBI energy.

3. RESULTS AND DISCUSSION

3.1. Potentiodynamic polarization behavior

The potentiodynamic polarization curves of steel by protection of PBI in sulfuric acid were shown in Figure 2. The corrosion current density values decrease significantly with the addition of PBI and the concentration increases. It can be found that the polarization curve of the cathodic branch decreases significantly, while the anodic branch change little. We think that PBI can adsorb on Fe surface, thereby inhibition of cathodic hydrogen evolution is significantly larger than the precipitation of anodic iron ions. The parallel trend of all cathodic polarization curves can be seen, which indicates that the reaction mechanism is not changed and PBI was geometrically covered on Fe surface [19-21].
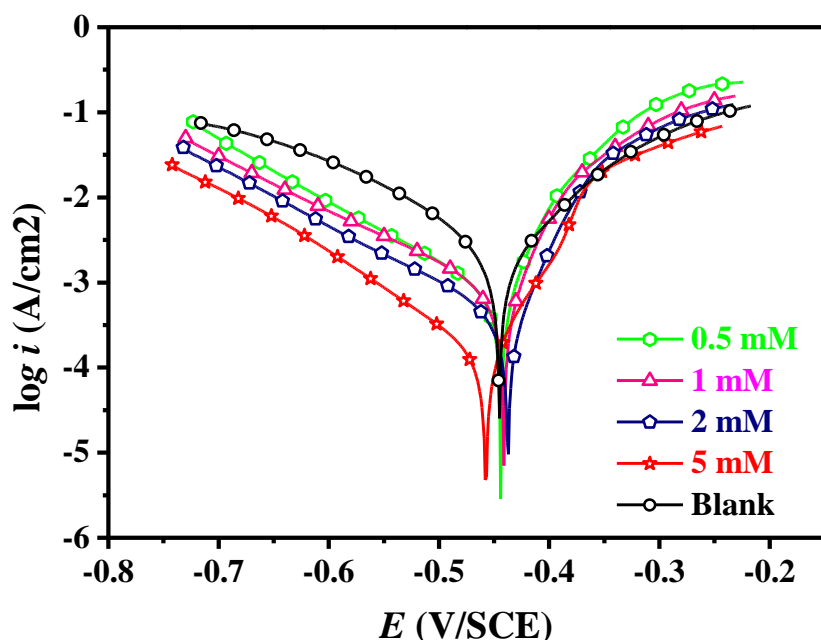
Figure 2. Polarization curves of steel by protection of different concentration of PBI in 0.5 M H_2SO_4 at 298 K.

Besides, we used Tafel extrapolation method to obtain electrochemical parameters including corrosion potential, corrosion current density, anodic and cathodic slope. The corrosion potential was −0.445 V in blank without added PBI, the corrosion potential gradually decreased with increasing PBI

concentration. It is worth mentioning that the change magnitude is significantly less than 85 mV, indicating the modest cathodic type of PBI for steel in H_2SO_4 [22]. Moreover, at concentration 5 mM, the η value is as high as 93.8%. This indicates that PBI can show great corrosion inhibition performance for X65 steel in sulfuric acid condition.

Table 1. Polarization parameters of steel in H_2SO_4 solution with protection of PBI at 298 K.

C (mM)	E_{corr}(V/SCE)	I_{corr}($\mu A\ cm^{-2}$)	β_c(mV dec^{-1})	β_a(mV dec^{-1})	η (%)
Blank	−0.445	2468	−143	99	—
0.5	−0.444	1169	−145	79	52.6
1	−0.441	897.6	−267	64	63.6
2	−0.437	580.6	−160	86	76.5
5	−0.458	153.6	−114	49	93.8

3.2. EIS
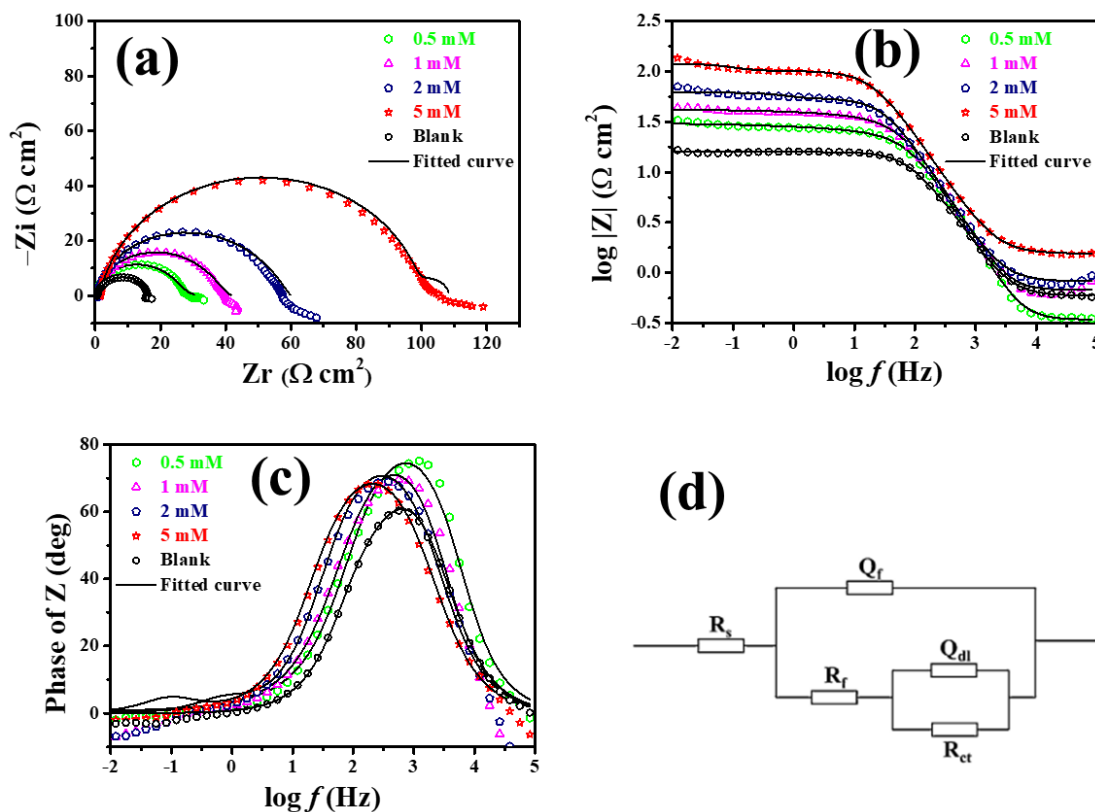
Figure 3. The Nyquist (a), Bode (b, c), and electrical circuit (d) images for steel with different concentrations of PBI in 0.5 M H_2SO_4 at 298 K.

Figure 3a shows Nyquist plots of PBI on steel in 0.5 M sulfuric acid. It is found that the radius of the capacitive loops arc increases significantly with increasing the concentration of PBI. This indicates the charge transfer resistance of steel increases, and thus increases the corrosion resistance of steel in H_2SO_4. Besides, all capacitive loops arcs are not a perfect semicircle, indicating that PBI adsorption on

steel surface lead to the surface uneven. We also find that all capacitive arcs shape did not change a lot, suggesting that the adsorption of PBI did not change relevant reaction mechanism of Fe [23, 24].

Figure 3b and c show impedance modulus and phase angle diagram of X65 steel with PBI in sulfuric acid, respectively. It can be seen that, as concentration of PBI increases, the phase angle diagram changes wider and higher, and the impedance mode value increases about an order of magnitude at low frequency region. This suggests the adsorption of PBI on steel strengths the anti-corrosion ability of Fe and thus PBI has excellent inhibition performance towards Fe in H_2SO_4.

The equivalent circuit diagram in Figure 3d was used to quantitative analysis to the inhibition ability of PBI. The fitted parameters are shown in Table 2. Herein, R_{ct} charge transfer resistance, R_s the solution resistance from SCE to steel electrode. R_f represents the film resistance. We find that R_{ct} value for blank solution is 12.2 Ω cm^2. As the concentration of ACBT increased to 5 mM, the R_{ct} value increases to 100.3 Ω cm^2. The inhibition efficiency at this time is as high as value of 87.8%, which is associated with potentiodynamic polarization results. We can also see C_{dl} value in blank is 278.0 μF cm^{-2}. The C_{dl} values have a downward trend with increasing the concentration of PBI and drops sharply to 79.3 and 10.3 μF cm^{-2} at 0.5 and 5 mM concentration. Helmholtz model can explain this phenomenon [25]:

$$C_{dl} = \frac{\varepsilon^0 \varepsilon}{d} S \qquad (7)$$

herein ε and ε^0 stand for the local and air dielectric constant, respectively, S is steel surface area, and d the thickness of the electric double layer. The PBI volume is obviously larger than that of water molecule and ε value of PBI is smaller than that of water molecule. When H_2O molecule on Fe surface were replaced by PBI, the ε^0 could become smaller and the thickness becomes larger. Thus, the value of C_{dl} decreases as the concentration of PBI increases.

Table 2. Impedance parameters of X65 steel in sulphric acid with protection of PBI at 298 K.

C (mM)	R_s (Ω cm^2)	R_f (Ω cm^2)	R_{ct} (Ω cm^2)	$Y_0 \times 10^{-6}$ (Ω^{-1} cm^{-2} s^n)	n	C_{dl} (μF cm^{-2})	η (%)
Blank	0.5	4.1	12.2	145.7	0.94	278.0	–
0.5	0.2	1.2	30.7	102.1	0.30	79.3	60.3
1	0.6	1.6	41.2	85.6	0.41	72.1	70.4
2	0.8	7.2	53.5	68.7	0.94	43.3	77.2
5	1.5	17.2	100.3	11.6	0.91	10.3	87.8

3.3. Weight loss measurement

As shown in Figure 4, the inhibition effect in 0.5 M H_2SO_4 containing different concentration PBI for steel was obtained. The results showed that increasing the concentration of PBI decreases the corrosion rate of X65 steel and increases inhibition efficiency up to a maximum value (92.1%) at 5 mM.

This inhibition behavior is consistent with results obtained from both electrochemical tests and indicates PBI is an effective corrosion inhibitor for steel in sulfuric acid.
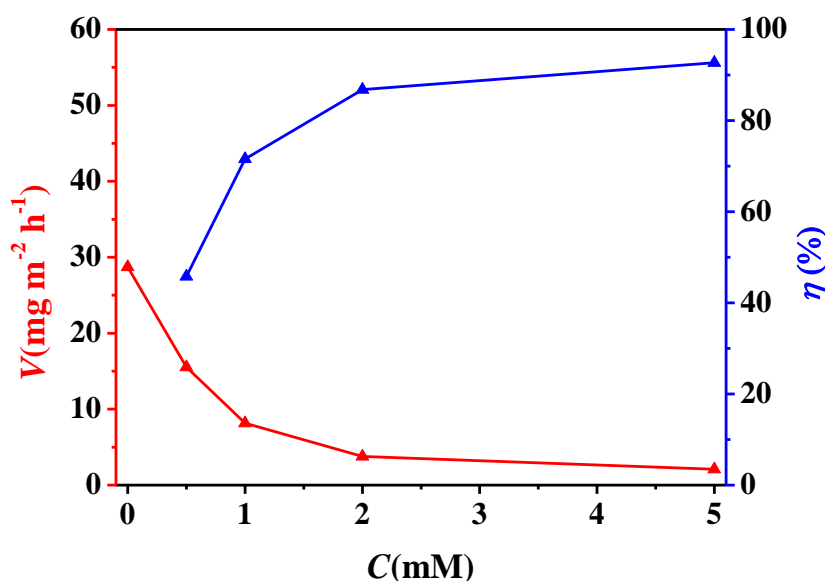
Figure 4. The weight loss graph of steel in 0.5 M H$_2$SO$_4$ at 298 K with different concentrations of PBI.

3.4. Langmuir analysis

Numerous adsorption isotherm models were used to explore the adsorption mechanism of PBI on steel. We used weight loss data to fit the adsorption model and find that the experimental conforms to Langmuir model, which can be expressed as follow [26]:

$$\frac{\theta}{1-\theta} = K_{ads}C \qquad (8)$$

$$K_{ads} = \frac{1}{55.5}\exp(-\frac{\Delta G_{ads}^0}{RT}) \qquad (9)$$

where K_{ads} stands for the adsorption equilibrium constant, ΔG_{ads}^0 stands for standard Gibbs energy, and θ stands for the coverage. The obtained Langmuir graph of straight line is shown in Figure 5. The fitted linear regression coefficient (R^2) is 0.9896, suggesting the fitting association is very well. It is generally accepted that the absolute ΔG_{ads}^0 value about −20 kJ mol^{-1} or lower indicate a physisorption, those in the order of −40 kJ mol−1 or higher involve charge sharing or a transfer, that is chemisorption [7, 27, 28]. The calculated values of standard free energy of adsorption ΔG_{ads}^0 is −31.2 kJ mol^{-1}. It is believed that PBI belongs to a mixed adsorption, that is chemical adsorption and physisorption are present meanwhile. In addition, negative ΔG_{ads}^0 value manifests that the adsorption of PBI on the surface of Q235 steel is autonomous process. Therefore, the ACBT adsorption on the surface of X65 steel belongs to the interaction of physicochemical adsorption. These result indicate the PBI film formation on the steel surface. This justifies the favorable inhibition ability of PBI towards Fe in H$_2$SO$_4$.
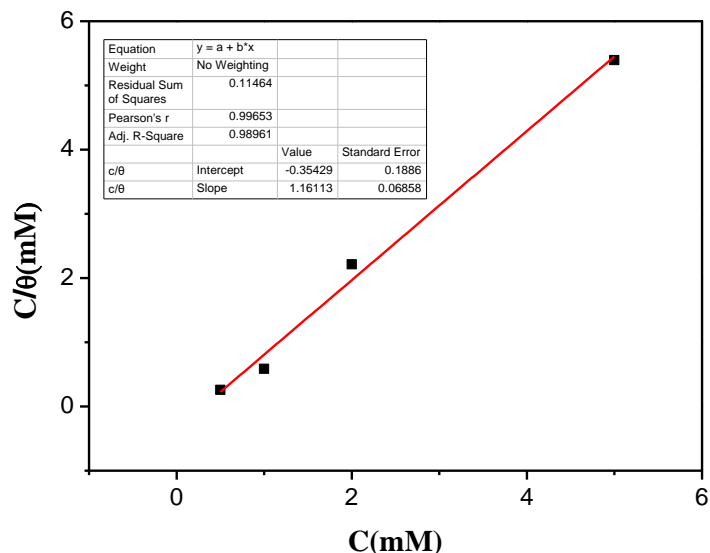
Equation	y = a + b*x		
Weight	No Weighting		
Residual Sum of Squares	0.11464		
Pearson's r	0.99653		
Adj. R-Square	0.98961		
		Value	Standard Error
c/θ	Intercept	-0.35429	0.1886
c/θ	Slope	1.16113	0.06858

Figure 5. Langmuir adsorption isotherm of steel in H_2SO_4 by the addition of PBI.

3.5. SEM observation

Figure 6 is SEM surface maps of steel samples immersed in H_2SO_4 solution at 298 K in the absence and presence of 5 mM PBI for 6 hours. For comparison, the SEM image of the freshly polished steel was also given. As seen in Figure 6a, the polishing stretches were visible on the surface of a freshly polished copper surface.
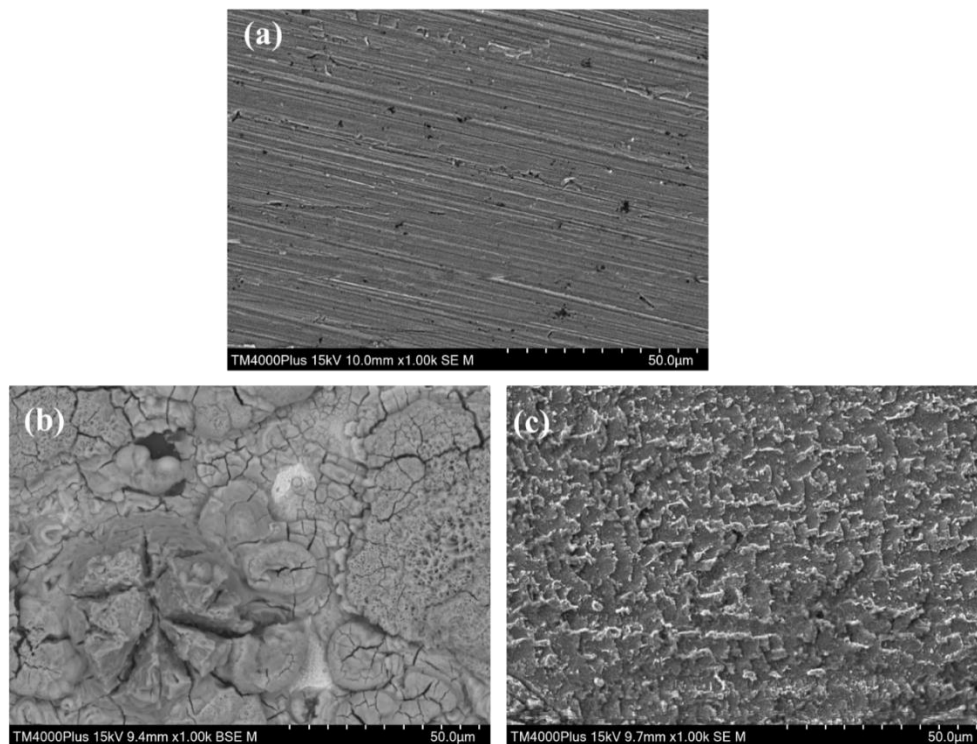

Figure 6. SEM images of polished steel (a), steel corroded in acid without (b) and with (c) protection of PBI in 0.5 M H_2SO_4 at 298 K.

The Fe surface after 6 h immersion was damaged with the attacking by H_2SO_4 without PBI. The corrosion products completely covered the surface. After addition the inhibitor PBI in 0.5 M H_2SO_4 solution (Figure 6c), there is no obvious corrosion holes on surface of steel. This strongly indicates that after adsorption on steel surface, PBI can remarkably suppress the steel corrosion in acid solution.

3.6. DFT calculation

In this work, DFT calculation of PBI was performed. The optimized molecular (a), HOMO (b), LUMO (c), Hirshfeld (d) and Mulliken (e) charges of PBI molecule are shown in Figure 7. The result of the calculation is presented in Figure 7. Frontier molecular orbital theory is a good way to study the chemical activity of organic compounds. As shown in Figure 7, the optimized molecular structure is planar construction, and HOMO and LUMO of PBI distributed on the whole molecule. It is favorable for parallel adsorption of PBI molecule on steel surface and thus a better inhibitive ability. Besides, it can be found that two N atom is negative charged in both Hirshfeld and Mulliken charge distribution, which indicates the charge transfer or sharing from N atoms in PBI molecule to Fe atoms. Therefore, the covalent bond is formed to fabricate the protective layer. In addition, the quantum chemical parameters energy gap ($\Delta E = E_{LUMO} - E_{HOMO}$) and dipole moment ($\mu$) were also obtained. The energy gap values of PBI is 2.68 eV, the small ΔE value indicates that organic inhibitor molecule has high inhibition performance for metal corrosion [29]. Workers believe large dipole moments correspond to excellent corrosion inhibition performance [30]. The dipole moment of PBI is 6.14 Debye, which can prove superior anti-corrosion performance of PBI.
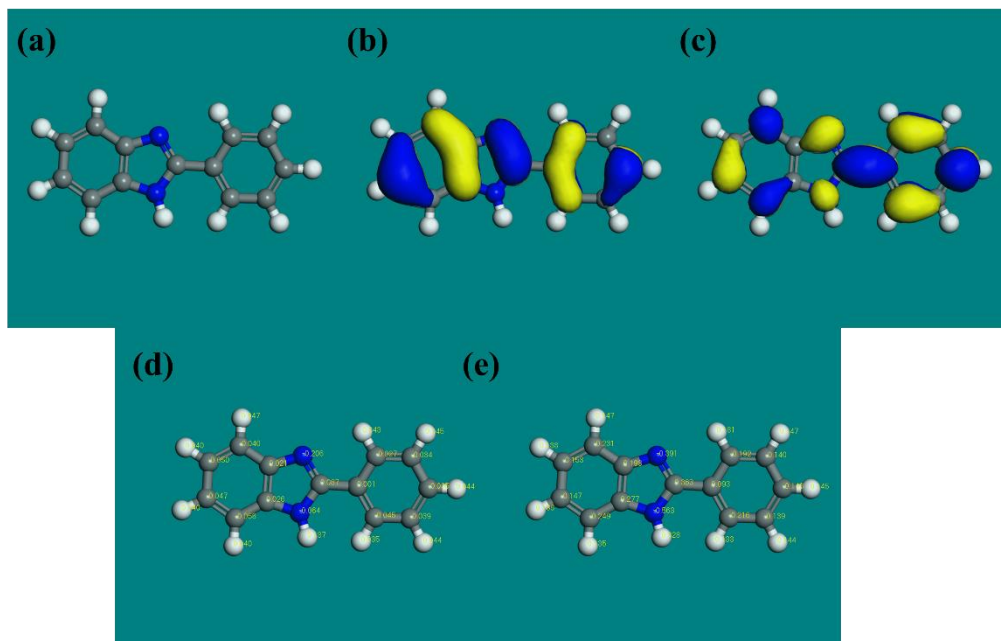
Figure 7. The optimized molecular (a), HOMO (b), LUMO (c), Hirshfeld (d) and Mulliken (e) charges of PBI molecule.

3.7. Molecular dynamics simulation

MDS was applied to evaluate the adsorption situation of PBI on Fe (110) surface. The obtained final snapshots of PBI over Fe (110) surface obtained from MDS are shown in Figure 8 (a) top view, without water molecules, (b) top view, with water molecules, (c) side view, without water molecules, (d) side view, with water molecules. We can see that PBI was adsorbed on Fe (110) surface in parallel mode in vacuum or solution environments. The maximum coverage of steel can be obtained to protect steel from acid attack, which is consistent with the results from quantum chemistry calculation. In addition, the binding energy values of PBI on Fe (110) are 213.4 kJ/mol and 261.2 kJ/mol under both vacuum and solution conditions respectively. Finally, we find that PBI has a powerful adsorption ability to Fe (110) surface, thereby excellent corrosion inhibition performance for steel in acid can be obtained.
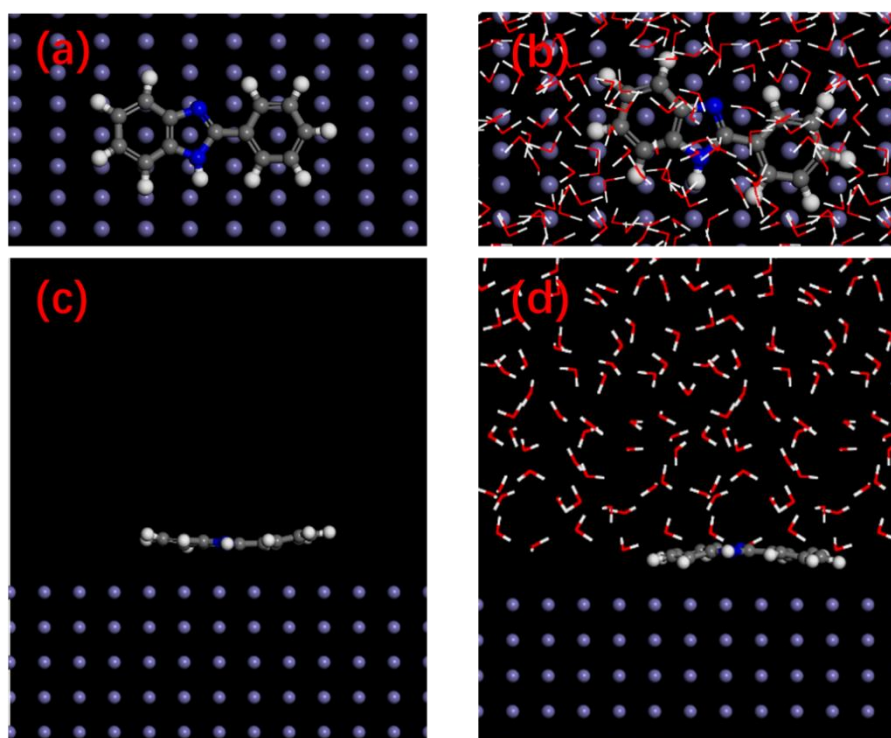
Figure 8. The final snapshots of PBI over Fe (110) surface obtained from MDS, (a) top view, without water molecules, (b) top view, with water molecules, (c) side view, without water molecules, (d) side view, with water molecules.

4. CONCLUSIONS

PBI was electrochemically and theoretically investigated as a high-efficiency corrosion inhibitor for X65 steel in 0.5 M H_2SO_4 medium. It can be found that PBI can only retard the cathodic reaction of steel, which is a modest cathodic type corrosion inhibitor. When the concentration of PBI is 5 mM at 298 K, its inhibition efficiency can reach to 93.8%. Surface morphology strongly support the analysis

results of electrochemical measurements. The adsorption behavior of PBI molecule on steel is consistent with Langmuir adsorption model. The adsorption type is a combination of physical and chemical adsorption. DFT calculations suggest the active adsorption sites of PBI molecule. Molecular dynamics simulation shows that PBI can adsorbs onto Fe(110) surface with a parallel mode, which can provide the largest protection area for X65 steel in acid solution.

References

1. Y. Qiang, S. Zhang, S. Xu, L. Guo, N. Chen, I.B. Obot, *Int. J. Electrochem. Sci.,* 11 (2016) 3147.
2. L. Guo, J. Tan, S. Kaya, S. Leng, Q. Li, F. Zhang, *J. Colloid. Interf. Sci.,* 570 (2020) 116.
3. M. Prabakaran, S.-H. Kim, N. Mugila, V. Hemapriya, K. Parameswari, S. Chitra, I.-M. Chung, *J. Ind. Eng. Chem.,* 52 (2017) 235.
4. M. Corrales-Luna, T. Le Manh, M. Romero-Romo, M. Palomar-Pardavé, E.M. Arce-Estrada, *Corros. Sci.,* 153 (2019) 85.
5. Y. Qiang, S. Fu, S. Zhang, S. Chen, X. Zou, *Corros. Sci.,* 140 (2018) 111.
6. E. A. Flores-Frias, V. Barba, M.A. Lucio-Garcia, R. Lopez-Cecenes, J. Porcayo-Calderon, J.G. Gonzalez-Rodriguez, *Int. J. Electrochem. Sci.,* 14 (2019) 5026.
7. H. M. Elabbasy, A. S. Fouda, *Int. J. Electrochem. Sci.,* 14 (2019) 3684.
8. A. S. Fouda, S. A. Abd El-Maksoud, A. El-Hossiany, A. Ibrahim, *Int. J. Electrochem. Sci.,* 14 (2019) 2187.
9. Y. Qiang, H. Li, X. Lan, *J. Mater. Sci. Tech.,* 52 (2020) 63.
10. B. Tan, S. Zhang, Y. Qiang, W. Li, H. Li, L. Feng, L. Guo, C. Xu, S. Chen, G. Zhang, *J. Mol. Liq.,* 298 (2020) 111975.
11. C. Monticelli, A. Balbo, J. Esvan, C. Chiavari, C. Martini, F. Zanotto, L. Marvelli, L. Robbiola, *Corros. Sci.,* 148 (2019) 144.
12. M. Murmu, K. Saha, N. Murmu, P. Banerjee, *Corros. Sci.,* 146 (2019) 134.
13. R. Sadeghi Erami, M. Amirnasr, S. Meghdadi, M. Talebian, H. Farrokhpour, K. Raeissi, *Corros. Sci.,* 151 (2019) 190.
14. Y. Qiang, S. Zhang, L. Guo, X. Zheng, B. Xiang, S. Chen, *Corros. Sci.,* 119 (2017) 68.
15. Y. Qiang, S. Zhang, S. Yan, X. Zou, S. Chen, *Corros. Sci.,* 126 (2017) 295.
16. Y. Qiang, S. Zhang, B. Tan, S. Chen, *Corros. Sci.,* 133 (2018) 6.
17. S.M. Tawfik, *J. Mol. Liq.,* 216 (2016) 624.
18. Y. Qiang, S. Zhang, L. Wang, *Appl. Surf. Sci.,* 492 (2019) 228.
19. Z. Xiao, Z. Zhou, L. Song, D. Wu, C. Zeng, Z. Cao, *Int. J. Electrochem. Sci.,* 14 (2019) 4705.
20. S. Y. Al-Nami, *Int. J. Electrochem. Sci.,* 14 (2019) 3986.
21. Y. Yang, Y. Li, L. Wang, H. Liu, D. Lu, L. Peng, *Int. J. Electrochem. Sci.,* 14 (2019) 3375.
22. Y. Qiang, S. Zhang, L. Guo, S. Xu, L. Feng, I.B. Obot, S. Chen, *J. Clean. Prod.,* 152 (2017) 17.
23. N. V. Likhanova, P. Arellanes-Lozada, O. Olivares-Xometl, I.V. Lijanova, J. Arriola-Morales, J. Mendoza-Hérnandez, *Int. J. Electrochem. Sci.,* 14 (2019) 2655.
24. C. Wang, W. Gou, C. Liu, D. Fu, L. Zhou, C. Lai, B. Xie, S. Zhu, *Int. J. Electrochem. Sci.,* 14 (2019) 3443.

25. Y. Qiang, S. Zhang, H. Zhao, B. Tan, L. Wang, *Corros. Sci.,* 161 (2019) 108193.
26. B. Tan, S. Zhang, Y. Qiang, L. Feng, C. Liao, Y. Xu, S. Chen, *J. Mol. Liq.,* 248 (2017) 902.
27. F. H. Al-abdali, M. Abdallah, R. El-Sayed, *Int. J. Electrochem. Sci.,* 14 (2019) 3509.
28. I. Martinović, G. Zlatić, Z. Pilić, L. Šušić, O. Kowalska, D. Petrović, F. Falak, J. Mišković, *Int. J. Electrochem. Sci.,* 14 (2019) 4206.
29. Y. Qiang, S. Zhang, S. Xu, W. Li, *J. Colloid. Interf. Sci.,* 472 (2016) 52.
30. L. Guo, S. Zhu, S. Zhang, Q. He, W. Li, *Corros. Sci.,* 87 (2014) 366